HHS Public Access

Author manuscript

Neuroimage. Author manuscript; available in PMC 2021 August 01.

Published in final edited form as:

Neuroimage. 2020 August 01; 216: 116791. doi:10.1016/j.neuroimage.2020.116791.

Concomitant Modulation of BOLD Responses in White Matter Pathways and Cortex

Arabinda Mishra[*,1,2], **Muwei Li**[1,2], **Adam W. Anderson**[1,2], **Allen T. Newton**[1,2], **Zhaohua Ding**[1,2], **John C. Gore**[1,2]

[1)]Department of Radiology and Radiological Sciences, Vanderbilt University Medical Center

[2)]Vanderbilt University Institute of Imaging Science, Vanderbilt University Medical Center

Abstract

In response to a flickering visual stimulus, the BOLD response in primary visual cortex varies with the flickering frequency and is maximal when it is close to 8Hz. In previous studies we demonstrated that BOLD signals in specific white matter (WM) pathways covary with the alternations between stimulus conditions in a block design in similar manner to gray matter (GM) regions. Here we investigated whether WM tracts show varying responses to changes in flicker frequency and are modulated in the same manner as cortical areas. We used a Fourier analysis of BOLD signals to measure the signal amplitude and phase at the fundamental frequency of a block-design task in which flickering visual stimuli alternated with blank presentations, avoiding the assumption of any specific hemodynamic response function. The BOLD responses in WM pathways and the primary visual cortex were evaluated for flicker frequencies varying between 2 and 14Hz. The variations with frequency of BOLD signals in specific WM tracts followed closely those in primary visual cortex, suggesting that variations in cortical activation are directly coupled to corresponding BOLD signals in connected WM tracts. Statistically significant differences in the timings of BOLD responses were also measured between visual cortex and specific WM bundles. These results confirm that when cortical BOLD responses are modulated by selecting different task parameters, relevant WM tracts exhibit corresponding BOLD signals that are also affected.

Keywords

White matter activation; BOLD; visual cortex; stimulus frequency

[*]Corresponding author: Arabinda Mishra, Vanderbilt University Institute of Imaging Science, Nashville, TN 37232, arabinda.mishra@vumc.org.

Credit Author Statement

Arabinda Mishra: Data curation and analysis, draft preparation. **Muwei Li**: Data acquisition and pre-processing. **Adam W. Anderson:** Methodology development. **Allen T. Newton:** Data acquisition and reviewing. **Zhaohua Ding:** Methodology writing, reviewing and editing. **John C. Gore:** Conceptualization, reviewing and supervision.

Introduction

Blood oxygenation level dependent (BOLD) contrast has for more than 25 years been exploited for detecting localized neural activity in the brain using fMRI. While BOLD signals have been robustly detected in gray matter (GM) in a very large number of studies, whether such signals reliably arise in white matter (WM) has been considered controversial (Gawryluk et al., 2014). Recently there have been a growing number of studies that strongly suggest that BOLD signals in WM encode neural activities and are measurable with conventional fMRI (Gore et al., 2019). For instance, Yarkoni et al. (2009) demonstrated that BOLD signal changes in WM could be detected with special task paradigms. Such functional activations of WM were later confirmed by Fabri et al. (2011), who mapped BOLD responses in the corpus callosum with a variety of sensory stimulations and motor tasks. We have more recently shown that sensory stimulations induce explicit BOLD responses along parts of the projection fiber pathways (Wu et. al., 2017), and that the induced BOLD changes covary with the temporal pattern of stimuli, just as GM. Furthermore, it has been found that the sensitivity of BOLD signal detection in WM increases at higher fields (Mazerolle et al., 2013) or by considering specific hemodynamic responses in WM (Courtmemanche et al., 2017).

In addition to the studies that involved explicit functional tasks or stimulations as above, it has been demonstrated that, using appropriate detection and analysis methods, BOLD effects are robustly detectable in a resting state as well although they are much weaker in WM. BOLD fluctuations in a resting state exhibit similar temporal and spectral profiles in both GM and WM (Ding et al., 2013), and their relative low frequency (0.01–0.08 Hz) signal powers are comparable (Ding et al., 2016). They also vary with baseline neural activity e.g. as induced by different levels of anesthesia in non-human primates (Wu et al., 2016).

In previous work (Ding et al., 2013; Ding et al., 2016) we reported that BOLD signals in WM in a resting state exhibit anisotropic temporal correlations with neighboring voxels. On the basis of these findings, we derived functional correlation tensors that quantify the correlational anisotropy in WM BOLD signals. We found that, along many WM tracts, the directional preferences of these functional correlation tensors in a resting state are grossly consistent with those revealed by diffusion tensors, and that external stimuli alter BOLD signals along specific task-relevant fiber pathways. These findings support the proposition that variations in WM BOLD signals are related to tract-specific neural responses, either intrinsic to WM or relaying effects from GM. We have more recently shown that sensory stimulations induce explicit BOLD responses along parts of the projection fiber pathways (Wu et. al., 2017), and that task-related BOLD changes covary with the temporal pattern of stimuli, just as GM. Thus there is converging and compelling evidence that WM exhibits both resting state fluctuations and stimulus-evoked BOLD signals very similar (Ding et al., 2018) to those in GM. A number of studies from other laboratories have also reported reliable observations of WM activations (Mazerolle et al., 2013; Gawryluk et al., 2009; Tettamanti et al., 2002; Yarkoni et al., 2009; Fabri et al., 2011; Weber et al., 2005; Astafiev et al., 2015).

Despite these findings, there remains a need for more conclusive evidence that BOLD effects in WM may be directly interpreted in terms of variations of intrinsic neural activity. Reports of successful demonstrations of activation-induced changes in WM to date are still quite sparse, and studies are needed that conclusively demonstrate direct relationships between GM activity and WM fMRI signals. For example, if BOLD signals from within WM are directly coupled to cortical neural activity, we hypothesize that, in a task that engages discrete cortical regions whose BOLD responses are known to be modulated by selecting different task parameters, relevant WM tracts should exhibit covarying BOLD signals that are also modulated. We report here our first results using such an approach.

Modulation of BOLD responses in the visual cortex by varying the frequency of flickering of a flashing checker-board, but keeping the stimulus on/off periods constant, was first reported by Thomas and Menon (1998) who measured the BOLD signal in primary visual cortex (V1). The BOLD response reached a maximum level when the flicker frequency was around 8 Hz and decreased at lower and higher values. Subsequent reports (Parkes et al., 2004; Singh et al., 2000; Singh et al., 2003; Srinivasan et al., 2007; Venkataraman et al., 2017) found similar results. In addition, the steady state visual evoked electrophysiological signal (SSVEP) was found to include a synchronized response at the same frequency as the flickering stimulus (Singh et al., 2003) which peaked at 10Hz (Herrmann, 2001), close to the peak BOLD and PET responses. Emir et al (2008) measured the effect of flicker frequency on the positive BOLD signal and the post stimulus undershoot (Emir et al., 2008) using a wider range of frequencies (1–44Hz) and confirmed peak activation in the visual cortex occurred at 8Hz. A recent measurement of the contrast sensitivity profile at four flicker frequencies (5:5:20Hz) in five retinotopically defined visual areas (Himmelberg and Wade, 2019) demonstrated that the response peaked at 10Hz, the closest frequency to 8Hz that was used . Thus it is clear that neural activity within visual areas can be modulated by the selection of the flickering frequency, with a peak around 8 Hz.

Our recent report of WM activation (Ding et al., 2018) showed that specific WM tracts showed BOLD signal variations with the same periodicity with cortical signals and a stimulus in a periodic block design. Huang et al (2018) subsequently showed that in the presence of a block-designed visual stimulus, WM voxels in specific areas showed signal variations at the stimulus frequency which could be identified by analyzing signal power spectra. WM regions responding to the stimulus produced signals with strong frequency components at the fundamental frequency of stimulation. To further demonstrate that such signals reflect the level of neural activity in cortical regions, we varied the flicker frequency of the visual stimulation presented and evaluated whether there were concomitant variations in both cortical and WM regions that would suggest a strong coupling between them. Signal changes in various WM regions were evaluated while varying the frequency of flicker from 2 to 14Hz. In addition, the phase differences of BOLD signal variations in various ROIs were also measured to evaluate their temporal relationships.

Material and Methods

Subjects and data acquisition:

FMRI data were acquired from fifteen healthy volunteers (mean age: 32 ± 9 years; range 21–53 years (7M/5F). None of the subjects had any history of neurological or psychiatric disorders determined by personal interview. The subject recruitment and fMRI data acquisition were carried out in accordance with protocols approved by the IRB (Institutional Review Board) of Vanderbilt University Medical Center. Seven sets of fMRI data were acquired from each subject in a single imaging session. Each subject was exposed to a visual stimulus consisting of a flashing checker-board reversing at a flicker frequency = 2, 4, 6, 8, 10, 12 or 14Hz. The flashing checker board was projected on to a screen mounted in the back of the scanner bore. Stimuli were presented in a block design with 20 s of stimulation alternating with 20 s of blank screen, repeated 6 times for each run. With TR=2 s, each run required 240 s and acquired 120 volumes. Different frequencies were presented in random order. Each stimulus cycle of 40s therefore corresponds to a fundamental frequency of stimulus = 0.025Hz.

FMRI and structural images of the brain were acquired with a 3T Philips Achieva scanner (Philips Healthcare, Inc., Best, Netherlands) using a 32-channel head coil at the Vanderbilt University Institute of Imaging Science. BOLD-sensitive functional images were obtained using a single shot T_2* weighted gradient echo, echo planar imaging (EPI) sequence (TR = 2s, TE = 45ms, matrix size = 80×80, FOV = 240×240mm^2, 43 axial slices each 3 mm thick, and 120 volumes) with voxel size 3×3×3mm. High resolution T_1-weighted images were acquired using a multi-shot, 3D gradient echo sequence (1×1×1mm^3 voxel size). Head motion during acquisition was minimized using a head restraining pad inside the head coil.

Pre-processing of fMRI time course

Standard pre-processing of fMRI and structural images was performed using SPM12 (http://www.fil.ion.ucl.ac.uk/spm) and custom codes in MATLAB. The T_2* weighted fMRI image sequences were slice time corrected followed by 3-D motion correction. Three out of fifteen subjects were excluded from the study based on motion criteria where the translation and rotation parameters measured during realignment were above a threshold limit (>2mm, >2^0). The T_1 weighted anatomic images were segmented (module: *Segment*) into WM and GM images and were subsequently co-registered with the mean, motion-corrected fMRI images. Finally, the processed functional and structural images for each subject were normalized into MNI (Montreal Neurological Institute, module*: Normalize*) template space. To minimize potential partial volume effects from nearby structures, the images were masked using a cut-off probability ($p > 0.8$) for GM and WM volumes, and stored separately to analyze regions of interest (ROIs). Spatial smoothing with a 6mm full-width at half maximum (FWHM) Gaussian kernel was performed separately within the WM and GM volumes of each subject to reduce noise. The JHU WM template (Oishi et al., 2009) in MNI space was used to identify ROIs as 48 segmented tracts. Only voxels belonging to both the WM mask and the selected ROIs were subsequently analyzed. The time course of each voxel was normalized by dividing by its standard deviation. The best straight line fit linear trend of the data was removed, resulting in a zero mean, unit variance signal, and each time series was then low

pass filtered using a Chebyshev type 2 filter with cut off 0.1Hz. Global signal changes were not removed from the fMRI time courses.

Analysis of frequency spectra of BOLD signal

There is ample evidence that the conventional hemodynamic response function (HRF) used to detect activation in GM is not suitable for WM, which tends to show a slower and delayed response (Li et al., 2019). We therefore used a Fourier analysis of each time series and examined the signal magnitude at the task frequency (0.025 Hz) as a measure of the response, which thus avoids assumptions about the precise shape of the HRF. The Fourier Transform was calculated of each processed time series (120 volumes spaced every 2s) which gave the magnitude of the signal at the task frequency for each voxel using a Fast Fourier transform (FFT). A map of signal magnitude at the stimulus frequency (MSF) was created for each subject. Similarly, the phase angle associated with the component at the task frequency, which measures the temporal delay in the BOLD response, was also obtained from the FFT. These data were then averaged across 12 subjects in MNI space, and the process was repeated for each flicker frequency 2 –14 Hz.

In order to identify WM voxels responding significantly to the visual stimulus, in each run we evenly split the six stimulus cycles into two halves (three cycles each, labelled A and B). The stimulus onsets in the two data sets are synchronized, so the summed signals (A+B) and their difference (A~B) were compared via an MWW (Mann Whitney Wilcoxon) test. This test distinguishes those voxels showing reliable activation from random noise effects. Only those voxels for which the MWW statistic was significant at $p<0.05$ level after Bonferroni corrections were retained for further analysis. The MSF associated with qualified voxels subjected to t-test were evaluated for each run (flicker frequency/task frequency) for individual subjects in the MNI space. The subject averaged MSF for corresponding frequency was then calculated for further analysis. For those significant voxels within each ROI, the MSF and associated phase delay at the task frequency (0.025 Hz) was calculated for each subject and then averaged across subjects for each flicker frequency. The fraction of responding voxels within each ROI was also calculated.

Analysis of white matter response to change in flicker frequency

The JHU WM template (Oishi et al., 2009) in MNI space comprises 48 segmented fiber bundles. The optic radiata (OR) in both hemispheres show the highest MSF at the task frequency. We selected four WM tracts besides OR, namely Splenium of corpus callosum (SCC), Middle cerebellar peduncle (MCP), Fornix (FXC) and Superior coronal radiata (SCR) based on previous reports of their functional involvements with visual tasks (e.g. Miller et al., 2015, Ding et al., 2018). Table 1 shows the mean MSF for each of these WM ROIs for those voxels satisfying the MWW test post correction. The t-statistics for each tract (ROI) considering the entire range of flicker frequencies are presented in the last column (Supplementary Data Table 1 contains the relevant data for 48 white matter bundles). The percentage signal changes (%S) in each stimulus cycle were also calculated relative to a baseline period i.e., six seconds prior to stimulation. However, the onset of activation in some ROIs occurred later in each cycle so %S were then calculated for intervals selected based of the pattern of activation. To describe the signals within each tract we fit the average

time courses of the percentage signal changes (%S) during a stimulus to a double gamma function. Table 2 shows the coefficients of the fits and delays to peak values associated with the first gamma function for the 5 tracts and the primary visual cortex.

Results

Stimulus evoked BOLD signals in gray and white matter.

Figure 1 shows the distribution of the normalized MSF to noise ratio at the fundamental frequency of the task (0.025 Hz) of the BOLD signals in gray and WM areas, for three different flicker frequencies, averaged across subjects in MNI space, and overlaid on representative T_1 weighted axial images. The subject-averaged mean signal to noise magnitudes were normalized to the peak value and thresholded (> 0.3) separately for GM and WM masks. Figure 1A shows MSF to noise ratio has a maximal value in the primary visual cortex (V1) and varied with the flicker frequency as seen in the different columns. Figure 1B shows the corresponding signal variations in the WM mask which can be seen to be distributed over various WM bundles. Figures 2A&B show the subject-averaged MSF to noise ratio versus the flicker frequency for all responsive voxels in GM and WM regions normalized to their peak values. The subject averaged voxel wise MSF for each stimulus frequency (2–14Hz) were normalized to the peak value in GM and WM mask separately. In both cases the peak signal occurs around 8Hz and decreases at lower and higher frequencies. The supplementary Figure 1 shows the similar frequency versus MSF relationships in visual cortex and five selected WM pathways considering ROIs in both hemispheres.

The average percentage signal changes within each period of stimulation were calculated relative to the baseline signal for each ROI. Figure 3a shows the percentage signal changes in the visual cortex (V1), optic radiata (OR) and splenium of corpus callosum (SCC) in the left hemisphere. The shaded area around the mean signal represents the standard deviation of signal in those voxels having at least 50% of the peak MSF in the ROIs at 0.025Hz. The blue, red and green curves represent the percentage signal changes at different flicker frequencies (4, 8 and 12Hz). There is clearly a variation in response to different frequencies with a peak percentage signal change occurring at 8Hz in both WM and GM. Supplementary figure 2 shows the lowpass filtered temporal signals from GM and two WM regions (cutoff 0.08Hz applying Chebyshev type 1) showing clear differences in phase relative to activation onset. The BOLD MSF % signal changes in V1 are approximately 8 times those in OR and other WM tracts show even smaller responses. The corresponding subject averaged power spectra in these bundles are shown in Figure 3B. The peak signal in WM showed the same variation with flicker frequency as seen in the visual cortex. Figure 3C shows the mean and standard error of the measurements of fractions of ROI volumes that showed significant responses. The mean value varies between 21 to 38%, which explains that the portion of ROI volumes sensitive to visual task is indicative of the effect. Supplementary figure 4 shows the responses in both GM and WM across several slices. The patterns of signal changes in specific white matter ROIs delineated in both hemispheres using the JHU template are presented in supplementary figure 5. The color scale is normalized to the peak subject averaged MSF. Given there is substantial difference in signal power at task frequency

between gray and white matter (Figure 3B) the color scaling for normalized the power better describes the signal change.

Difference in temporal variation of BOLD response in white matter bundles.

Figure 4 shows the BOLD signal responses averaged over all cycles of the stimulus in visual cortex and WM areas, along with their fits to double gamma functions. The mean and standard error (shaded envelop) of the double gamma fitted response curves for various WM bundles show that their response patterns are different from that of the GM response and from each other. Tables 2A&B show the magnitude coefficients and delays for each ROI. However, most WM pathways show a more complex signal response with a considerable delay in their response patterns so the gamma fits do not capture this complexity well. Figure 4 and Table 2 compare the fits for three flicker frequencies (4, 8 and 12Hz). The WM response to 8Hz shows the largest magnitude and qualitatively appeared to show the shortest delay to peak in some tracts. All the response fitting was performed based on ROIs in the left hemisphere only. However, we also found similar changes in the right hemisphere (data not shown). Although the t-statistics of a few ROIs have large values, only the data in selected bundles are presented in this work.

The phase angle associated with the fundamental frequency of the BOLD signal was calculated to estimate the time delay in BOLD responses for the six GM and WM regions and the results are shown in Figure 5. The Whisker boxplots in Figure 5A–C show the distribution of phase angles (measured in terms of delay in seconds) associated with the stimulus frequency (0.025Hz) for flicker frequencies 4, 8 and 12Hz. One-way ANOVA was used to test the statistical significance of measured differences between all possible combinations of ROI pairs. A statistically significant difference between V1 and four WM bundles (OR, SCC, MCP & SCR) but not FXC was observed (p value <0.01, corrected for multiple comparisons) at 4 or 8Hz flicker frequency. However, we did not detect any differences in delay time between V1 and FXC for any rate of flicker in the entire range 2–14Hz. The outliers, the values two standard deviation away from mean value on either side, were not considered for statistical analysis. The standard deviation of phase angles across subjects was measured to quantify the inter-subject variation of parameters. Figure 5D shows the matrix of standard deviations representing the time delays associated with all six ROIs for the entire range of flicker frequencies. The overall variance is observed to be smaller in V1 and SCC compared to other areas, whereas the signal variation is smallest at 8Hz for most ROIs compared to other frequencies. We noticed maximum variation of delay (phase angle) in FXC in comparison to the other WM bundles. Figure 6 shows the subject averaged phase map overlaid on the visual cortex and OR (A, B) in four representative slices (8hz, flicker frequency), which indicates an increasing delay from anterior to direction. The magnified images (C, D) on identical slice locations shows a detailed view.

Discussion:

Major findings

By varying the flicker frequency over the range 2 to 14Hz, we demonstrated that the magnitudes of the BOLD responses in selected WM bundles, as well as in primary cortical

regions, change with rate of flicker in similar manner. The optic radiata (OR) showed the largest signal at the task frequency, and this varied with flicker rate in similar manner to GM. Supplementary figure 3 shows the double gamma fitted activation responses for each flicker frequency. SCC showed a significant signal change, but the temporal response was different and characterized by a large decrease in signal prior to a later increase. The time delays of the BOLD responses in most WM bundles were significantly delayed compared to those in visual cortex. We emphasize that the complex waveforms seen in e.g. Figure 4 represent the summed signals from entire tracts. If, as seems likely, the signal at each segment along a tract is delayed significantly, then such patterns may be expected even if the response at any single segment is simpler.

Although it has been controversial whether WM activation is robustly detectable using fMRI (Logothetis and Wandell, 2004; Grajauskas et al., 2019), activations of relevant WM regions by visual stimulations have been consistently reported to date (Mazerolle et al., 2008; Gawryluk et al., 2009; Gawryluk et al. 2011). It was found that, similar to the findings from this work particularly with an 8 Hz flicker frequency, the hemodynamic response in WM exhibits a reduced peak amplitude (Fraser et al., 2012) and delayed peak time (Courtemanche et al., 2018), which may be accounted for by the distinct hemodynamic environment that WM experiences (Li et al. 2019).

Distributions of frequency responses in WM (supplementary data table 1) show that the majority of fiber pathways exhibited a peak MSF at 8Hz, whether or not they are directly associated with the visual system. It is also noticed a significant portion of ROIs ($t > 3$) had stronger responses to frequencies other than 8Hz where nearly half of them responded strongest to 6Hz (e.g., OR_L). The responses at 8Hz across the majority of WM tracts were presumably attributable to global responsiveness of the brain to visual stimulations. Indeed, it has been observed that brain responses extend well beyond the areas of primary relation to the task (Gonzalez-Castillo et al., 2012). Although the study was performed on GM under optimal noise conditions, phenomena of similar nature should exist in WM as well even under an increased noise level. Of note, the observed peak MSF at frequencies other than 8Hz was likely due to noise artifacts in WM.

While in keeping well with the literature reports, the findings from this study should be interpreted with caution. First, the number of subjects studied was relatively small, which limited the signal-to-noise ratio in the WM BOLD signals observed. Second, there is a common concern in studies of BOLD effects in WM with potential contamination due to partial volume averaging (PVA) with GM. Although care was taken to avoid this potential confound, residual PVA effects might arise from imperfect processing procedures such as errors in co-registration, though these seem unlikely in deep regions of larger tracts. Also, BOLD effects in WM are potentially caused by venous drainage from activated cortical regions. This could account for the delays in signal changes, but as pointed out by (Huang et al., 2018), the cortex and deep WM are drained by two distinct venous systems with opposite draining directions (Rui'z et al., 2009), so that it is unlikely that the observed BOLD effects in WM were all driven by "upstream" GM under physiological conditions.

Task specificity of WM responses

The OR is the WM pathway connecting the lateral geniculate nuclei of the thalamus to the primary visual cortex that transmits visual information from the eyes. Task specific BOLD signals in this pathway shows similar characteristics as those in the primary visual cortex (V1) (Fig. 3A and Fig. 4A&B), but with smaller magnitudes that vary with flicker frequency in the same way as cortex. The SCC contains WM pathways that are involved in coordinating visual activities inter-hemispherically (Knyazeva MG, 2013), and the FXC has been found to be implicated in visual memory (Miller et al., 2015). The MCP is formed by fibers connecting the cerebellum and the pontine nuclei, to which the main inputs arise from the cerebral cortical areas that convey eye motion-related information (Glickstein and Voogd, 2011). In the meantime, the corona radiata has been previously shown to be involved in eye movement as well (Sherrington, 1894).

Time delay in BOLD response

Stimulus driven BOLD responses in GM are normally characterized by a standard hemodynamic response function (HRF) that is used as a predictor in General Linear Model analyses. However, the HRF for WM is different and variable so that it is inappropriate to use the canonical HRF to detect activation. We used a Fourier analysis of the signal time courses which assumes only that the BOLD response is periodic at the same frequency as the task stimulus. We did not evaluate the signals at any other frequencies than the fundamental, which reduces sensitivity but is an unbiased approach for evaluating the signal magnitude and phase. The time delays measured by the corresponding signal phase were statistically significantly different from GM in various WM bundles. The mean and median phase differences suggest that there is roughly 2–3s delay in BOLD responses between four WM bundles (OR, SCC, MCP and SCR) and V1. This delay is essentially consistent for most flicker frequencies.

Throughout the analysis we considered the amplitude and phase of the BOLD signal to be functionally homogeneous within each WM tract. The phase angles in each WM tract appear to be distributed over a range and to be more variable than in GM. This variation may be due to the lower BOLD signals in WM and the effects of noise or it may reflect an intrinsic functional heterogeneity of the WM bundles e.g. at different depths. The estimated magnitude and delay parameters using two gamma fitting (Li et al., 2019) in Table 2 gives an idea of overall signal magnitude (MSF) and time delay of the mean response in ROIs at 8Hz flicker frequency. However, the signal delay calculated using FFT in Figure 5 shows the distribution of delays associated with individual voxels in the ROIs. We did not see strict similarity between the mean (green dots, fig5A–C) and table 2 due to the obvious difference in parameter estimations using gamma fit and FFT. Additionally, gamma fitting was performed after evaluating the mean signal, while the delays using FFT were calculated on a voxel by voxel basis. Indeed, future studies at higher resolution and signal to noise ratio may allow more detailed evaluation of the variation of timing differences along tracts. As illustration, Figure 6 shows the estimated phase delays voxel-by-voxel along the OR. There is an apparent monotonic increase in the delay in an inferior-posterior direction, consistent with a blood supply provided by the middle and posterior cerebral arteries.

Overall these studies add to the growing evidence that BOLD signals may be evoked in WM in response to a stimulus, that they are task-specific in different areas, and that their magnitudes covary with the level of neural activity and corresponding BOLD signals in cortical regions to which they connect. The effects extend over distances much larger than might be easily explained by drainage effects from cortex to adjacent WM regions, and thus suggest that these BOLD effects reflect an intrinsic functional response within WM.

Supplementary Material

Refer to Web version on PubMed Central for supplementary material.

Acknowledgements

This work was supported by NIH grant R01 NS093669 (J.C.G).

References

Astafiev SV, Shulman GL, Metcalf NV, Regachary J, MacDonald CL, Harrington DL, Maruta J, Shimony JS, Ghajar J, Diwakat M, Huang MX, Lee RR, Corbetta M, 2015 Abnormal white matter blood-oxygen-level-dependent signals in chronic mild traumatic brain injury. J Neurotrauma, 32(16), 1254–71. [PubMed: 25758167]

Azevedo FAC, Carvalho LRB, Grinberg LT, Farfel JM, Ferretti REL, Leite REP, Jacob W, Lent R, Herculano-Houzel S, 2009 Equal Numbers of Neuronal and Nonneuronal Cells Make the Human Brain an Isometrically Scaled-Up Primate Brain. Journal of Comparative Neurology 513, 532–541. [PubMed: 19226510]

Courtemanche MJ, Sparrey CJ, Song X, MacKay A, D'Arcy RC, 2018 Detecting white matter activity using conventional 3 Tesla fMRI: An evaluation of standard field strength and hemodynamic response function. Neuroimage 169:145–150. [PubMed: 29229580]

Ding ZH, Huang YL, Bailey SK, Gao YR, Cutting LE, Rogers BP, Newton AT, Gore JC, 2018 Detection of synchronous brain activity in white matter tracts at rest and under functional loading. Proceedings of the National Academy of Sciences of the United States of America 115, 595–600. [PubMed: 29282320]

Ding ZH, Newton AT, Xu R, Anderson AW, Morgan VL, Gore JC, 2013 Spatio-Temporal Correlation Tensors Reveal Functional Structure in Human Brain. PLoS One 8.

Ding ZH, Xu R, Bailey SK, Wu TL, Morgan VL, Cutting LE, Anderson AW, Gore JC, 2016 Visualizing functional pathways in the human brain using correlation tensors and magnetic resonance imaging. Magnetic Resonance Imaging 34, 8–17. [PubMed: 26477562]

Dolan RJ, 2008 Neuroimaging of cognition: past, present, and future. Neuron 60, 496–502. [PubMed: 18995825]

Emir UE, Bayraktaroglu Z, Ozturk C, Ademoglu A, Demiralp T, 2008 Changes in BOLD transients with visual stimuli across 1–44 Hz. Neuroscience Letters 436, 185–188. [PubMed: 18400397]

Fabri M, Polonara G, Mascioli G, Salvolini U, Manzoni T, 2011 Topographical organization ofhuman corpus callosum: an fMRI mapping study. Brain Research 1370:99–111. [PubMed: 21081115]

Fox MD, Raichle ME, 2007 Spontaneous fluctuations in brain activity observed with functional magnetic resonance imaging. Nat Rev Neurosci 8, 700–711. [PubMed: 17704812]

Fraser LM, Stevens MT, Beyea SD, D'Arcy RC, 2012 White versus gray matter: fMRI hemodynamic responses show similar characteristics but differ in peak amplitude. BMC Neurosci. 8 1;13:91. [PubMed: 22852798]

Gawryluk JR, D'Arcy RC, Mazerolle EL, Brewer KD, Beyea SD, 2011 Functional mapping in the corpus callosum: a 4T fMRI study of white matter. Neuroimage, 54(1):10–5. [PubMed: 20643213]

Gawryluk JR, Brewer KD, Beyea SD, D'Arcy RCN, 2009 Optimizing the detection of white matter fMRI using asymmetric spin echo spiral. Neuroimage 45, 83–88. [PubMed: 19084071]

Gawryluk JR, Mazerolle EL, D'Arcy RCN, 2014 Does functional MRI detect activation in white matter? A review of emerging evidence, issues, and future directions. Frontiers in Neuroscience 8.

Glickstein M, Sultan F, Voogd J, 2011 Functional localization in the cerebellum. Cortex. 47:59–80. [PubMed: 19833328]

Gore JC, Gao Y, Rogers BP, Anderson AW, Huang Y, Mishra Arabinda, Newton AT, Schilling KG, Wu TL, Li M, Chen LM, and Ding Z, 2019 "Functional MRI and Resting State Connectivity in White Matter – a mini-Review", Magnetic Resonance Imaging, 63:1–11 [PubMed: 31376477]

Grajauskas LA, Frizzell T, Song X, 2019 D'Arcy RCN. White Matter fMRI Activation Cannot Be Treated as a Nuisance Regressor: Overcoming a Historical Blind Spot. Front Neurosci. 10 4;13:1024. [PubMed: 31636527]

Gonzalez CJ, Saad ZS, Handwerker DA, Inati SJ, Brenowitz N, and Bandetttini PA, 2012 Whole-brain, time-locked activation with simple task revealed using massive averaging and model-free analysis. PNAS. 109(14):5487–92. [PubMed: 22431587]

Helenius J, Perkio J, Soinne L, Ostergaard L, Carano RAD, Salonen O, Savolainen S, Kaste M, Aronen HJ, Tatlisumak T, 2003 Cerebral hemodynamics in a healthy population measured by dynamic susceptibility contrast MR imaging. Acta Radiologica 44, 538–546. [PubMed: 14510762]

Herrmann CS 2001 Human EEG responses to 1–100 Hz flicker: resonance phenomena in visual cortex and their potential correlation to cognitive phenomena. Experimental Brain Research 137, 346–353. [PubMed: 11355381]

Himmelberg MM, Wade AR, 2019 Eccentricity-dependent temporal contrast tuning in human visual cortex measured with fMRI. Neuroimage 184, 462–474. [PubMed: 30243956]

Hoeft F, Barnea-Goraly N, Haas BW, et al. 2007 More is not always better: increased fractional anisotropy of superior longitudinal fasciculus associated with poor visuospatial abilities in Williams syndrome. The Journal of Neuroscience. 27(44):11960–11965. [PubMed: 17978036]

Huang Y, Bailey SK, Wang P, Cutting LE, Gore JC, Ding Z, 2018 Voxel-wise detection of functional networks in white matter. Neuroimage 183, 544–552. [PubMed: 30144573]

Huttunen JK, Grohn O, Penttonen M, 2008 Coupling between simultaneously recorded BOLD response and neuronal activity in the rat somatosensory cortex. Neuroimage 39, 775–785. [PubMed: 17964186]

Kastner S, O'Connor DH, Fukui MM, Fehd HM, Herwig U, Pinsk MA, 2004 Functional imaging of the human lateral geniculate nucleus and pulvinar. J Neurophysiol 91, 438–448. [PubMed: 13679404]

Knyazeva MG 2013 Splenium of corpus callosum: Patterns of interhemispheric interaction in children and adults. Neural Plast. 2013:639430.

Leopold DA, Maier A, 2012 Ongoing physiological processes in the cerebral cortex. Neuroimage 62, 2190–2200. [PubMed: 22040739]

Logothetis NK, Wandell BA, 2004 Interpreting the BOLD signal. Annu Rev Physiol 66, 735–769. [PubMed: 14977420]

Li M, Newton AT, Anderson AW, Ding Z, Gore JC, Characterization of hemodynamic response function in white matter tracts for event-related fMRI. Nature Comunications. https://www.nature.com/articles/s41467-019-09076-2.

Mazerolle EL, D'Arcy RC, Beyea SD, 2008 Detecting functional magnetic resonance imaging activation in white matter: interhemispheric transfer across the corpus callosum. BMC Neurosci. 9 12;9:84.

Mazerolle EL, Gawryluk JR, Dillen KN, Patterson SA, Feindel KW, Beyea SD, Stevens MT, Newman AJ, Schmidt MH, D'Arcy RC, 2013 Sensitivity to white matter FMRI activation increases with field strength. PLoS One 8, e58130.

Miller JP, Sweeta JA, Bailey CM, Munyon CN, Luders HO, Fastenuau PS, 2015 Visual-spatial memory may be enhanced with theta burst deep brain stimulation of the fornix: A preliminary investigation with four cases. Brain 138:1833–1842. [PubMed: 26106097]

Ogawa S, Tank DW, Menon R, Ellermann JM, Kim SG, Merkle H, Ugurbil K, 1992 Intrinsic Signal Changes Accompanying Sensory Stimulation - Functional Brain Mapping with Magnetic-Resonance-Imaging. Proceedings of the National Academy of Sciences of the United States of America 89, 5951–5955. [PubMed: 1631079]

Oishi K, Faria A, Jiang HY, Li X, Akhter K, Zhang JY, Hsu JT, Miller MI, van Zijl PCM, Albert M, Lyketsos CG, Woods R, Toga AW, Pike GB, Rosa-Neto P, Evans A, Mazziotta J, Mori S, 2009 Atlas-based whole brain white matter analysis using large deformation diffeomorphic metric mapping: Application to normal elderly and Alzheimer's disease participants. Neuroimage 46, 486–499. [PubMed: 19385016]

Parkes LM, Fries P, Kerskens CM, Norris DG, 2004 Reduced BOLD response to periodic visual stimulation. Neuroimage 21, 236–243. [PubMed: 14741661]

Preibisch C, Haase A, 2001 Perfusion imaging using spin-labeling methods: Contrast-to-noise comparison in functional MRI applications. Magnetic Resonance in Medicine 46, 172–182. [PubMed: 11443724]

Rosen BR, Savoy RL, 2012 fMRI at 20: Has it changed the world? Neuroimage 62, 1316–1324. [PubMed: 22433659]

Sherrington CS (1894) Experimental note on two movements of the eye. Journal of Physiology. 17(1–2): 27–29.

Ruıź D, Yilmaz Ha, Gailloud P (2009) Cerebral developmental venous anomalies: current concepts. Annals of neurology 66:271–283. [PubMed: 19798638]

Singh KD, Smith AT, Greenlee MW, 2000 Spatiotemporal frequency and direction sensitivities of human visual areas measured using fMRI. Neuroimage 12, 550–564. [PubMed: 11034862]

Singh M, Kim S, Kim TS, 2003 Correlation between BOLD-fMRI and EEG signal changes in response to visual stimulus frequency in humans. Magnetic Resonance in Medicine 49, 108–114. [PubMed: 12509825]

Srinivasan R, Fornari E, Knyazeva MG, Meuli R, Maeder P, 2007 fMRI responses in medial frontal cortex that depend on the temporal frequency of visual input. Experimental Brain Research 180, 677–691. [PubMed: 17297549]

Tettamanti M, Paulesu E, Scifo P, Maravita A, Fazio F, Perani D, Marzi CA, 2002 Interhemispheric transmission of visuomotor information in humans: fMRI evidence. J Neurophysiol 88:1051–1058. [PubMed: 12163553]

Thomas CG, Menon RS, 1998 Amplitude response and stimulus presentation frequency response of human primary visual cortex using BOLD EPI at 4 T. Magnetic Resonance in Medicine 40, 203–209. [PubMed: 9702702]

Venkataraman AP, Lewis P, Unsbo P, Lundstrom L, 2017 Peripheral resolution and contrast sensitivity: Effects of stimulus drift. Vision Research 133, 145–149. [PubMed: 28268102]

Weber B, Treyer V, Oberholzer N, Jaermann T, Boesiger P, Brugger P, Regard M, Bulk A, Savazzi S, Marzi CA, 2005 Attention and interhemispheric transfer: a behavioral and fMRI stiudy. J Cogn Neurosci, 17(1), 113–23. [PubMed: 15701243]

Wu TL, Wang F, Anderson AW, Chen LM, Ding ZH, Gore JC, 2016 Effect of Anaesthesia on resting state BOLD signal in white matter of non-human primates. Magnetic resonance Imaging 9, 1235–41

Wu X, Yang Z, Bailey SK, Zhou J, Cutting L,E, Gore JC, Ding ZH, 2017 Functional connectivity and activity of white matter in somatosensory pathways under tictile stimulations. Neuroimage 152, 371–80. [PubMed: 28284801]

Yarkoni T, Barch DM, Gray JR, Conturo TE, Braver TS, 2009 BOLD correlates of trial-by-trial reaction time variability in gray and white matter: a multi-study fMRI analysis. PLoS One 4:e4257.

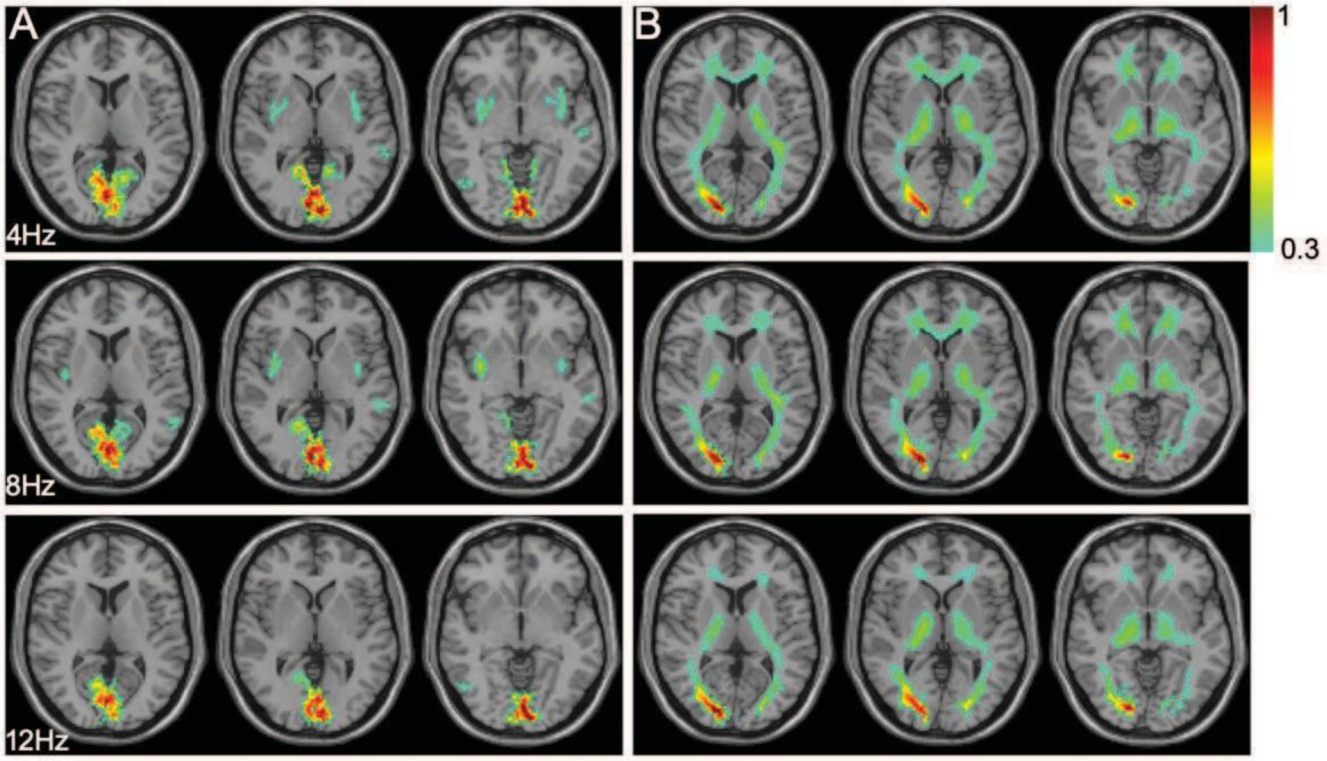

Figure 1. Magnitude of signal to noise ratio at stimulus frequency in GM and WM.

(A) The normalized ratio of GM signal magnitude to noise at stimulus frequency (0.025Hz) overlaid on anatomic images. Rows refer to signal magnitude at 4, 8 and 12 Hz on three representative slices containing BA17&18. Color scale represents the variation of subject averaged normalized signal at stimulus frequency (>0.3). (B) Similar WM map overlaid on anatomic images to compare signal magnitudes.

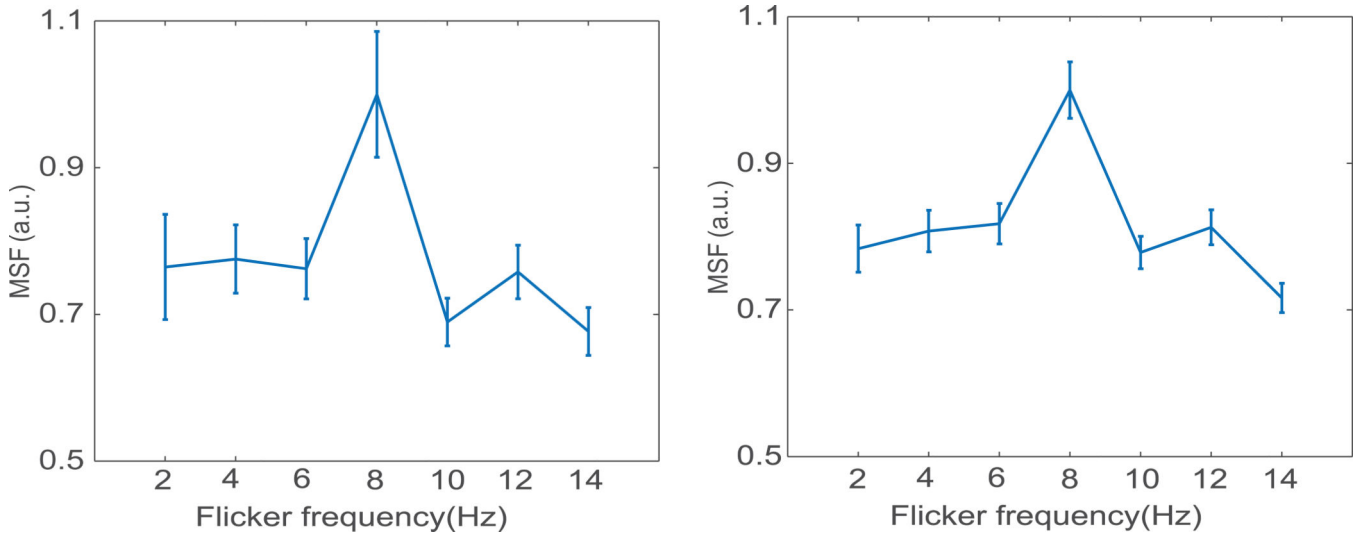

Figure 2. Signal magnitude at stimulus frequency (MSF) to noise ratio vs. flicker frequency.

(A) Subject averaged normalized MSF to noise ratio and the standard error versus the flicker frequency in the gray matter (2:2:14Hz, $p<0.05$). (B) Similar normalized MSF to noise ratio calculated for the WM mask versus the frequency range. The subject averaged signal magnitude for each stimulus frequency were normalized to the peak value in GM and WM mask separately.

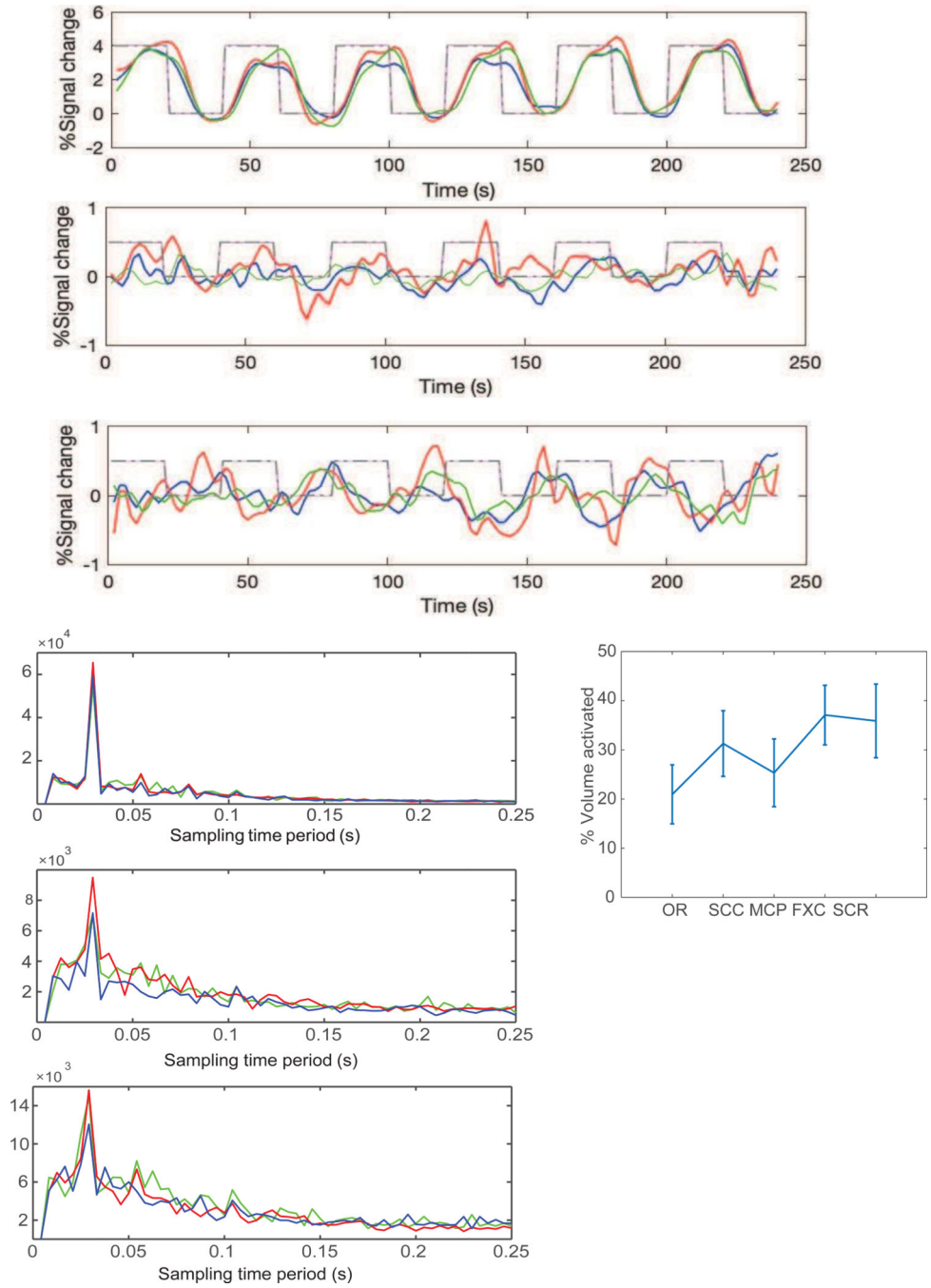

Figure 3. Percentage signal change (PSC) and power spectral density (PSD).

(A) percentage signal change in visual cortex (V1, top), optic radiata (OR, middle) and splenium of corpus callosum (SCC, bottom) at flicker frequency 4Hz (blue), 8Hz (red) and 12Hz (green). The dotted steps in the background represents the stimulus on/off cycle during acquisition in seconds. (B) Power spectral density in the corresponding ROIs where color represents the flicker frequency of stimulus (time course of representative voxels after Bonferroni correction).Mean and standard error plot showing percentage volume activated in various white matter ROIs.

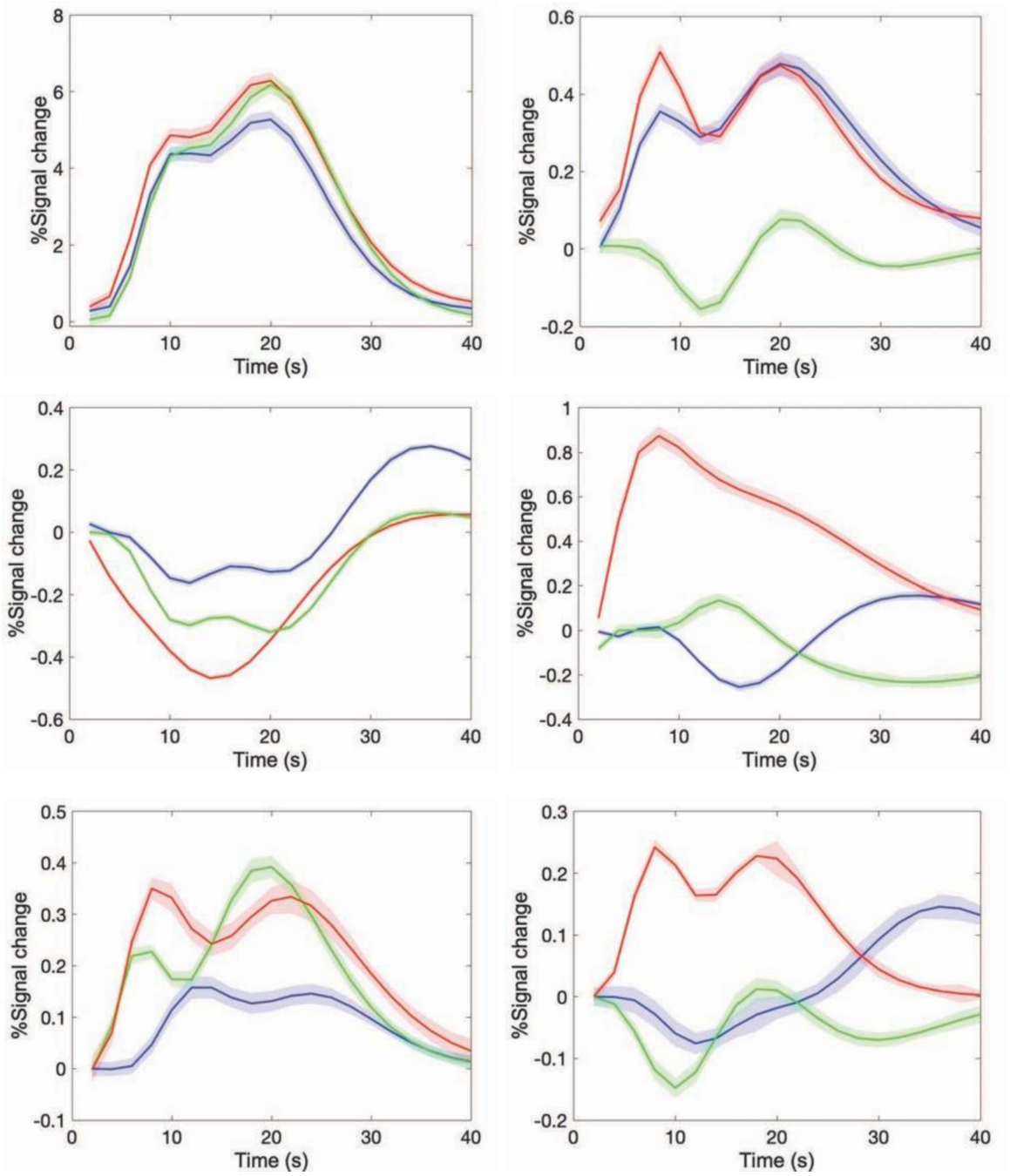

Figure 4. Stimulus response at various GM and WM bundles.

Cycle averaged stimulus response (fitted with double gamma function) of gray mater activation (V1) and five white matter bundles. The estimated percentage signal change and corresponding standard error (shaded band) refers to 4 (blue), 8(red) and 12Hz (green) flicker frequency in the Brodman's area (V1, A), Optic-radiata (OR, B), Splenium of corpus callosum (SCC, C), Middle cerebellar peduncle (MCP, D), Fornix (FXC, E) and Superior coronal radiata (SCR, F).

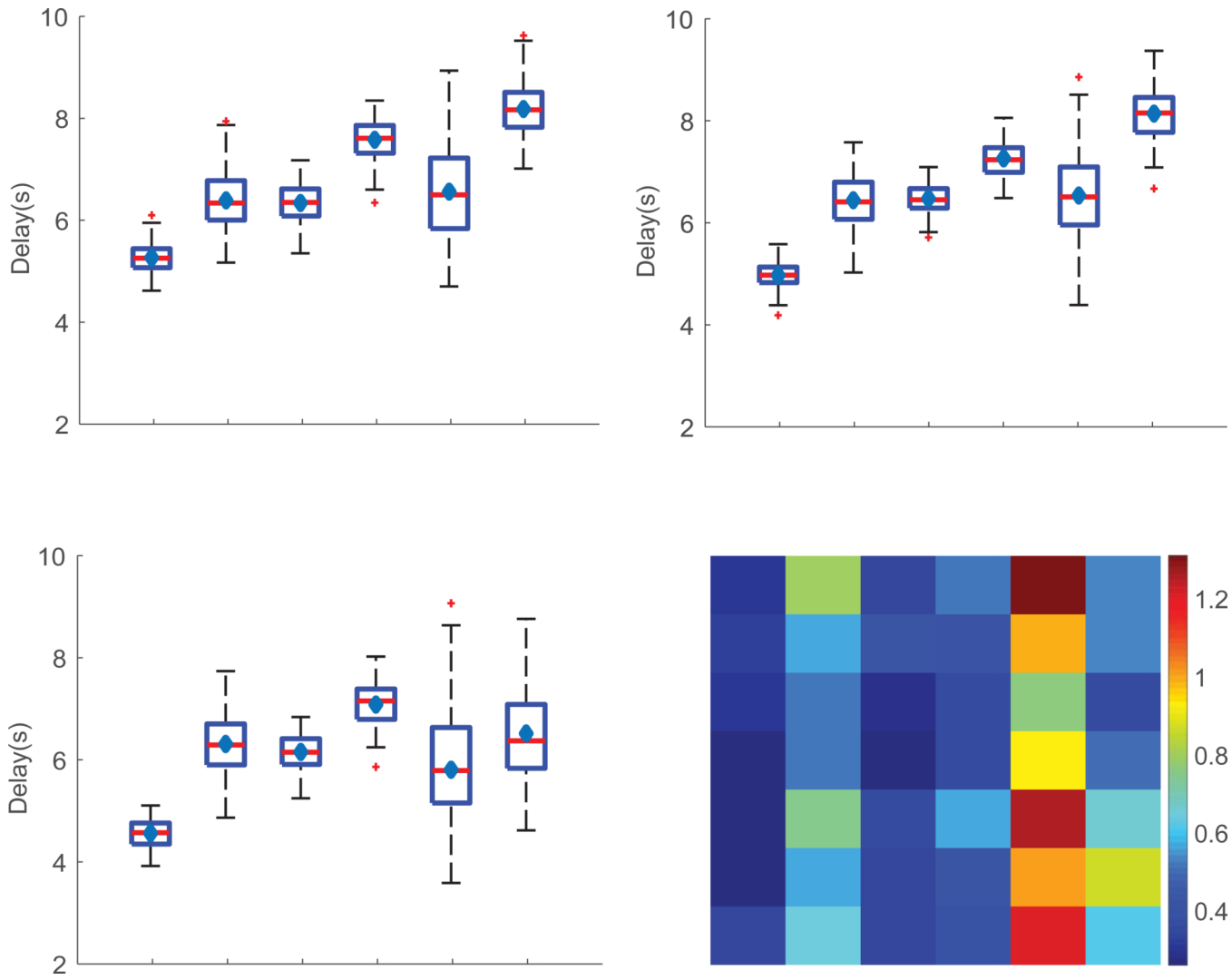

Figure 5. Activation delay in GM and WM bundles.

(A-C) Whisker boxplot showing the delay in BOLD response (phase angle from signal Fourier Transform) measured in seconds for GM (BA) and WM (OR, SCC, MCP, FXC, SCR) bundles at flicker frequency 4Hz (A), 8Hz (B) and 12Hz (C). Red horizontal lines and blue diamond shapes inside the box refers to the mean and median value of phase lag. (D) Matrix plot showing the standard deviation of delay(s) associated with each ROI over the entire range of flicker frequency.

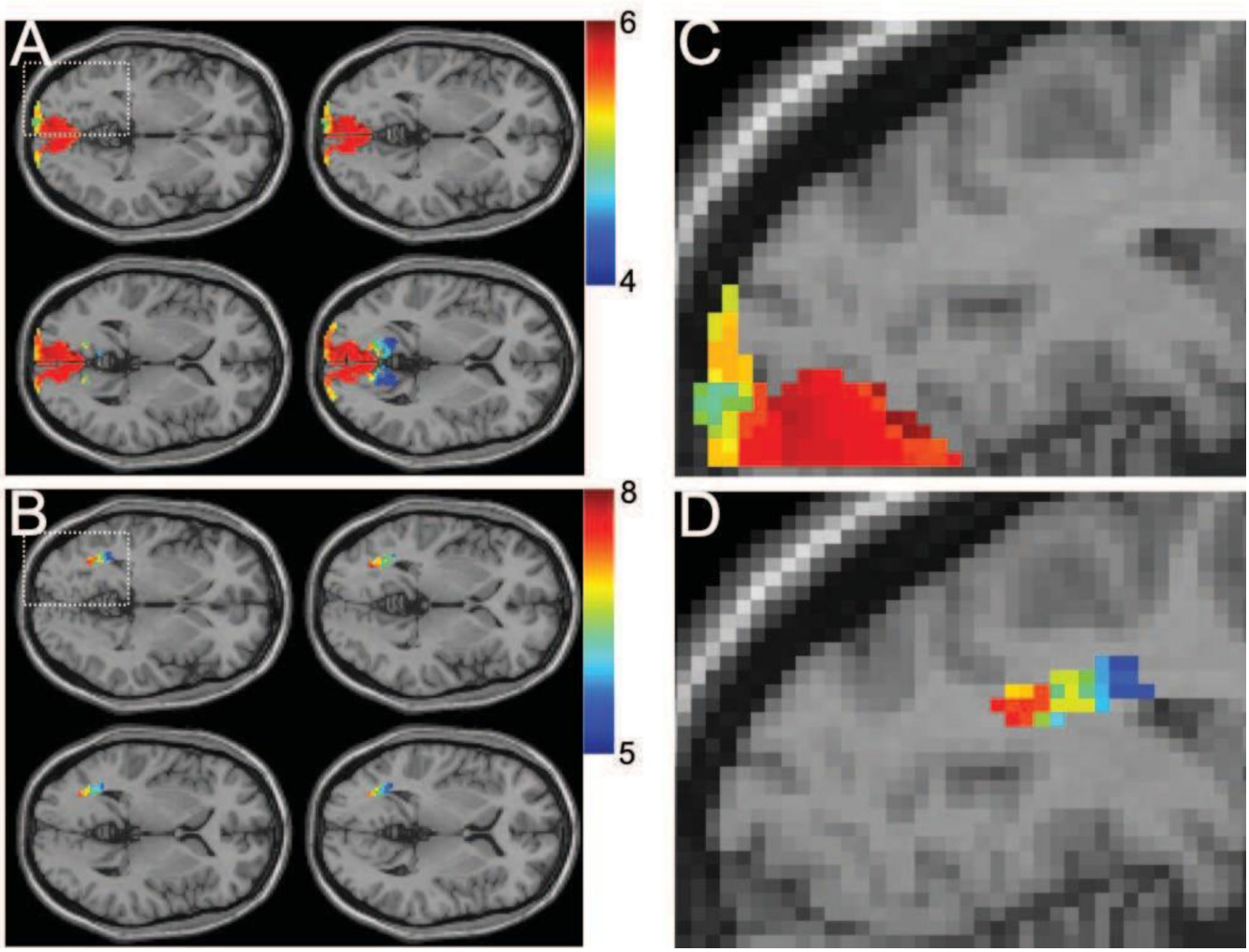

Figure 6. Phase delay in stimulus activation.

(A, B) Phase delay map for BA (SLN 6) and OR (SLN −2) overplayed on anatomic map ($p < 0.05$, corrected). (C, D) Magnified view of activation in the left hemisphere for a representative slice. *SLN: slice number in MNI space.

Table 1

Subject averaged MSFx1000($p<0.05$, corrected)

	2hz	4hz	6hz	8hz	10hz	12hz	14hz	t
1. OR_R	7.4143	4.006	7.6361	9.7718	7.5702	9.3905	5.8857	8.9752
OR_L	3.8757	3.4649	7.8571	4.9304	5.5656	6.8958	3.9173	7.3855
2. Splenium_of_corpus_callosum	4.9022	3.4328	5.1236	4.0813	2.0733	3.5478	5.7504	7.4192
3. Middle_cerebellar_peduncle	1.5649	3.5851	2.6184	4.6601	1.3766	1.7752	2.6661	4.3798
4. Fornix_Stria_terminalis_R	3.5923	2.839	3.8937	4.7832	1.2206	3.0204	1.0668	5.3706
Fornix_Stria_terminalis_L	1.6783	1.6497	1.8364	3.0633	1.7153	1.1256	1.2989	3.7259
5. Superior_corona_radiata_R	3.4769	3.013	6.0142	1.3715	3.1259	0.6871	1.9802	4.1075
Superior_corona_radiata_L	1.649	1.4149	4.0639	3.327	1.5965	1.5456	0.7986	3.8846

Column-1–7. Subject averaged mean MSF (2:2:14Hz, $p<0.05$, corrected) calculated for ROIs (OR, SCC, MCP, FXC & SCR). Column 8, The t-score considering the MSF in each bundle associated with the entire range of flicker frequencies (df = 11)

Table 2A.

Amplitude coefficient of 1st gamma function

	BA	OR	SCC	MCP	FXC	SCR
4HZ	3.2030	0.0753	0.0231	0.1495	0.1921	0.0811
8HZ	3.9975	0.1304	0.1811	0.8709	0.5685	0.2851
12HZ	3.0698	0.0860	0.2071	0.0626	0.4331	0.0664

Table 2B.

Time delay (seconds) associated with the overshoot in double gamma fitting

	BA	OR	SCC	MCP	FXC	SCR
4HZ	2.0006	2.2592	8.7720	4.2592	2.3311	9.1883
8HZ	2.0000	2.0003	3.7468	2.4540	2.1546	4.1377
12HZ	2.0000	6.9200	2.0031	9.2153	6.6160	2.0012